

A strategy to search for an inner binary black hole from the motion of the tertiary star

TOSHINORI HAYASHI ¹, SHIJIE WANG ¹ AND YASUSHI SUTO ^{1, 2}

¹*Department of Physics, The University of Tokyo, Tokyo 113-0033, Japan*

²*Research Center for the Early Universe, School of Science, The University of Tokyo, Tokyo 113-0033, Japan*

(Received 2019 December 4; Revised 2020 January 10; Accepted 2020 January 18)

ABSTRACT

There are several on-going projects to search for stars orbiting around an invisible companion. A fraction of such candidates may be a triple, instead of a binary, consisting of an inner binary black hole (BBH) and an outer orbiting star. In this paper, we propose a methodology to search for a signature of such an inner BBH, possibly a progenitor of gravitational-wave sources discovered by *LIGO*, from the precise radial velocity (RV) follow-up of the outer star. We first describe a methodology using an existing approximate RV formula for coplanar circular triples. We apply this method and constrain the parameters of a possible inner binary objects in 2M05215658+4359220, which consists of a red giant and an unseen companion. Next we consider co-planar but non-circular triples. We compute numerically the RV variation of a tertiary star orbiting around an inner BBH, generate mock RV curves, and examine the feasibility of the BBH detection for our fiducial models. We conclude that the short-cadence RV monitoring of a star-BH binary provides an interesting and realistic method to constrain and/or search for possible inner BBHs. Indeed a recent discovery of a star-BH binary system LB-1 may imply that there are a large number of such unknown objects in our Galaxy, which are ideal targets for the methodology proposed here.

Keywords: techniques: radial velocities - celestial mechanics - (stars:) binaries (including multiple): close - stars: black holes

1. INTRODUCTION

The first direct detection of a gravitational wave (GW) from a binary black-hole (BBH) merger (Abbott et al. 2016) has convincingly established the presence of very compact BBHs in the universe. While the origin, evolution and distribution of such BBHs are not yet understood, several interesting scenarios have been proposed so far. The binary evolution scenario (e.g. Belczynski et al. 2002, 2007, 2012, 2016; Dominik et al. 2012, 2013; Kinugawa et al. 2014, 2016; Spera et al. 2019) assumes that a fraction of massive stars form binary systems, experiences supernovae, and finally evolves into compact binaries including BBHs. The dynamical formation scenario, on the other hand, considers

that stars and BHs located in dense clusters experience significant gravitational interactions, and eventually form BBHs ejected from the cluster regions mainly through binary-single, in addition to binary-binary, scattering encounters (e.g. Portegies Zwart & McMillan 2000; O’Leary et al. 2009; Rodriguez et al. 2016; Tagawa et al. 2016). The primordial BH scenario (e.g. Sasaki et al. 2016, 2018; Bird et al. 2016) proposes that numerous primordial BHs are formed in the very early universe and a tiny fraction of them experiences close encounter and forms tight BBHs through the GW emission.

Regardless of such different formation scenarios, however, there should be a much more abundant population of their progenitor BBHs. Since those BBHs would have wider separations and thus longer orbital periods, they do not generate a detectable GW signal, except for the last few seconds before the final merger. Also they are difficult to be directly imaged unless they are surrounded by appreciable accretion disks. Therefore, the presence of such unseen binaries have to be searched for through their dynamical influence on nearby visible objects, including a radial velocity variation of an outer tertiary star due to the inner BBH. Such a detection is challenging, but if successful, it will not only constrain the formation and evolutionary channel towards the GW emitting BBHs, but also establish a yet unknown class of exciting astrophysical objects.

Indeed there exist a couple of known interesting systems that are relevant for such a strategy. One is a triple system consisting of a white dwarf-pulsar binary and an outer white dwarf orbiting around the inner binary (Ransom et al. 2014). The system was detected with the arrival time analysis of the pulsar. Quite interestingly, the inner and outer orbits of the triple system are near-circular and coplanar; the eccentricities of the inner and outer orbits are $e_{\text{in}} \sim 6.9 \times 10^{-4}$ and $e_{\text{out}} \sim 3.5 \times 10^{-2}$, and their mutual inclination is $i = (1.20 \pm 0.17) \times 10^{-2}$ deg.

The other is a red giant 2M05215658+4359220 with an unseen massive object of $\sim 3M_{\odot}$, possibly a BH or even a neutron star binary (Thompson et al. 2019). The system was discovered from a systematic survey of stars exhibiting anomalous accelerations. The follow-up radial-velocity (RV) observation indicates that the orbit is also near-circular; $e_{\text{out}} = 0.00476 \pm 0.00255$. These two examples are very encouraging, implying that the dynamical search for unseen companions of visible objects is very rewarding.

A very recent discovery of a star–BH binary system, LB-1, by Liu et al. (2019) is added in the above list. Later, Abdul-Masih et al. (2019) and El-Badry & Quataert (2019) pointed out that the mass of the inner BH would plausibly be $5M_{\odot} \lesssim M \lesssim 20M_{\odot}$, much smaller than the original claim of $\sim 70M_{\odot}$ by Liu et al. (2019). In addition, Shen et al. (2019) put a strong constraint on the presence of an inner BBH for LB-1. Nevertheless, it is very encouraging in a sense that such a new population of star-BH binary systems in a nearly circular orbit really exists, perhaps abundantly in our Galaxy.

Indeed, there are several on-going/future projects that search for unseen companions around stars. *Gaia* was launched at the end of 2013, and performs astrometric survey for a billion of stars in the Galaxy. Since the astrometry of *Gaia* has great precision especially for bright stars, it can detect a subtle motion of a star around an unseen object. Therefore, in addition to the survey of stellar binaries (e.g. El-Badry & Rix 2018; Ziegler et al. 2018), there are many proposals to search for star – BH binaries with *Gaia* (e.g. Breivik et al. 2017; Kawanaka et al. 2017; Mashian & Loeb 2017; Yamaguchi et al. 2018). Yamaguchi et al. (2018), for instance, estimate that *Gaia* can detect 200 – 1000 binaries in its 5 year operation considering the binary evolution scenario.

Additionally, *TESS* launched in 2018 is carrying out a photometric survey of nearby stars to search for transit planets. Masuda & Hotokezaka (2019) conclude that *TESS* will potentially discover $\mathcal{O}(10)$

binaries consisting of a star and an unseen compact object through identifying relativistic effects in their photometric light-curves, for instance.

Thus it is quite likely that *Gaia*, *TESS* and other surveys will detect many binary systems with an unseen object. Given the LIGO discovery of very tight BBHs, it is natural to expect that a fraction of those systems are indeed triple systems that host unseen inner BBHs. Therefore it is important to see if one can dynamically distinguish between a single BH and a binary BH in such triple systems. In addition, the stellar evolution of multiple systems is still poorly understood. Future detection of a triple with an inner BBH would shed light on dynamical processes in triple evolution (e.g. [Toonen et al. 2016](#); [Hamers et al. 2013](#); [Stephan et al. 2016](#)).

In this paper, we propose a methodology to search for an inner BBH in a triple system from the short-term outer stellar RV variations due to inner BBH perturbation through intensive RV monitoring (see Figure 1). Interestingly, such RV variations were first considered by [Schneider & Cabrera \(2006\)](#) in a context of a possible degeneracy between an inner binary and an S-type circumbinary planet. Later, [Morais & Correia \(2008\)](#) derived an analytic perturbative formula for RV variations in a coplanar circular triple, and pointed out that the inner binary model produces two nearby but distinct frequency modes around twice its orbital frequency. If the two modes can be identified separately, the degeneracy with the planet model, which produces a single frequency mode, can be broken in principle. Their work is further extended for eccentric and inclined triples by ([Morais & Correia 2011](#)).

Such approximate analytic formulae are very useful in understanding the origin and parameter dependence of the RV variations, but they neglect the back-reaction on the inner BBH by the outer orbit. Therefore accurate numerical simulations are needed for broader and more realistic configurations of such triples. This is what we conduct in what follows. We also generate mock RV curves, and discuss the observational feasibility for our fiducial model.

The rest of the paper is organized as follows. In section 2, we first summarize the analytic approximation RV formula for a coplanar circular triple by [Morais & Correia \(2008\)](#), and explain features of the RV variations induced by an inner unseen binary. As a specific application of the formula, we constrain a possible inner binary in a star–unseen-object binary system 2M05215658+4359220. Section 3 introduces a set of fiducial triple configurations. In particular, we focus on a coplanar circular triple, and present a methodology to search for an inner BBH through the RV curves computed numerically. Section 4 applies the methodology for coplanar eccentric triples, and discusses the observational feasibility through mock observations. We discuss how to break the degeneracy of the RV variations due to circumbinary planets and the inner BBHs. Finally, section 6 summarizes and concludes this paper. Appendix presents a detailed derivation of an analytic approximation formula by [Morais & Correia \(2008\)](#) and the parameter degeneracy of the RV variations in the S-type planet and the inner BBH models.

2. RADIAL-VELOCITY VARIATION FOR A COPLANAR CIRCULAR TRIPLE

In this section, we first present an approximation formula for RV variations for a coplanar circular triple with an inner binary, which was derived by [Morais & Correia \(2008\)](#). This analytic formula is useful to show basic feature of RV variations, and also to estimate the expected amplitude of RV variations in designing an RV followup strategy discussed in the next section. As a specific application for that purpose, we put a constraint on a possible inner binary in a binary system

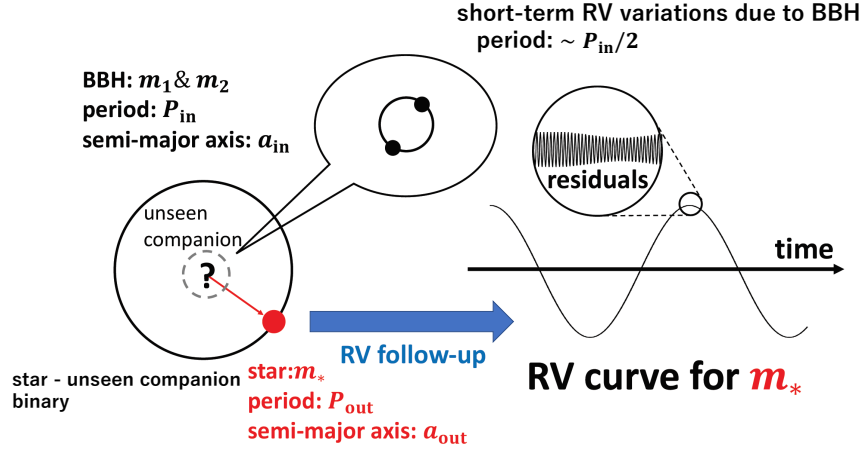


Figure 1. A schematic illustration for a methodology to search for inner BBHs using the RV variation of a tertiary star.

2M05215658+4359220. For definiteness, we summarize a derivation of the approximate formula in appendix A.

2.1. Analytic approximation formula

We consider a coplanar circular hierarchical triple consisting of an inner binary and a star. The RV of the tertiary star orbiting around the inner binary (Morais & Correia 2008) is given by

$$\begin{aligned}
 V_{\text{RV}} \approx & K_0 \left[1 + \frac{3}{4} \left(\frac{a_{\text{in}}}{a_{\text{out}}} \right)^2 \frac{m_1 m_2}{(m_1 + m_2)^2} \right] \sin I \cos[\nu_{\text{out}} t + \theta_0] \\
 & - \frac{15}{16} K_{\text{BBH}} \sin I \cos[(2\nu_{\text{in}} - 3\nu_{\text{out}})t + (2S_0 - \theta_0)] \\
 & + \frac{3}{16} K_{\text{BBH}} \sin I \cos[(2\nu_{\text{in}} - \nu_{\text{out}})t + (2S_0 + \theta_0)],
 \end{aligned} \tag{1}$$

where I is the inclination of the stellar orbit axis with respect to the line of sight, ν_{in} and ν_{out} are mean motions of the inner and outer orbits, and S_0 and θ_0 are constant phases specified by the initial conditions.

The first term in the right-hand-side of equation (1) corresponds to the Keplerian motion of the star. The semi-amplitude of the unperturbed Keplerian RV for a edge-on view is given by

$$K_0 \equiv \frac{m_1 + m_2}{m_1 + m_2 + m_*} a_{\text{out}} \nu_{\text{out}}, \tag{2}$$

where m_1 , m_2 and m_* are the masses of the inner binary and the outer star, and a_{out} is the semi-major axis of the stellar orbit. For further detail, see appendix A.

The second and third terms express the RV variations induced by an inner binary. The semi-amplitude of the variations is proportional to K_{BBH} defined as

$$K_{\text{BBH}} \equiv \frac{m_1 m_2}{(m_1 + m_2)^2} \sqrt{\frac{m_1 + m_2 + m_*}{m_1 + m_2}} \left(\frac{a_{\text{in}}}{a_{\text{out}}} \right)^{3.5} K_0 \tag{3}$$

parameter	value	meaning
P_{out}	83.205 ± 0.064 days	orbital period
m_{co}	$3.3_{-0.7}^{+2.8} M_{\odot}$	mass of an unseen companion
m_{giant}	$3.2_{-1.0}^{+1.0} M_{\odot}$	mass of a red giant
e_{out}	0.00476 ± 0.00255	eccentricity
ω_{out}	197.13 ± 32.07 deg	argument of pericenter
$\sin i$	$0.97_{-0.12}^{+0.03}$	inclination of the orbital plane
R_{giant}	$30_{-6}^{+9} R_{\odot}$	radius of a red giant

Table 1. Best-fit parameters for the binary system 2M05215658+4359220 (Thompson et al. 2019)

with a_{in} being the semi-major axis of the inner binary.

Equation (1) indicates that the RV variations due to an inner binary consist of two periodic terms with frequencies of $2\nu_{\text{in}} - \nu_{\text{out}}$ and $2\nu_{\text{in}} - 3\nu_{\text{out}}$. Since we consider a system with $\nu_{\text{in}} \gg \nu_{\text{out}}$, K_{BBH} is much smaller than K_0 by a factor of $(a_{\text{in}}/a_{\text{out}})^{3.5}$, and their frequencies are well approximated by $2\nu_{\text{in}}$. Thus it is not easy to identify the two distinct modes observationally.

Morais & Correia (2008) pointed out, however, that the separation of the two modes is crucial to distinguish the RV variation of the inner binary against a single periodic modulation induced by a planet orbiting the star. Morais & Correia (2011) extended this consideration for eccentric and inclined cases using a perturbation theory.

The above result shows that a planet around a star in a binary system produces a signal very similar to that expected for an inner binary in a triple system. We discuss the degeneracy between the two models in section 5. In turn, a detection of an inner binary requires a well-organized observational monitor with short-cadence as we discuss below.

2.2. Constraint on a binary system 2M05215658+4359220

Thompson et al. (2019) reported a discovery of a binary system 2M05215658+4359220 that consists of a red giant and an unseen massive object. They first searched for systems exhibiting anomalously large radial accelerations from the Apache Point Observatory Galactic Evolution Experiment (APOGEE) radial velocity data, and selected 200 candidates of such binaries. After checking the photometric variations from the All-Sky Automated Survey for Supernovae (ASAS-SN) data, they identified 2M05215658+4359220 as the most likely binary candidate. Subsequently, they performed the radial velocity follow-up observation with the Tillinghast Reflector Echelle Spectrograph (TRES) on the 1.5 m telescope at the Fred Lawrence Whipple Observatory (FLWO). They obtained 11 spectra with the precision of about 0.1 km s^{-1} over several months in 2017 and 2018.

Interestingly, the orbital period of the system turned out to be very close to that of the photometric variation of the star, indicating the tidal synchronization. Therefore they assume that the inclination of the rotation axis of the outer red giant i_{rot} is equal to its orbital inclination i_{orb} with respect to the line of sight: $i \equiv i_{\text{rot}} = i_{\text{orb}}$. This enabled them to estimate the best-fit parameters of the system (Table 1) from the RV data and the spectroscopic analysis of the red giant.

Thompson et al. (2019) estimated the mass of the unseen companion to be $m_{\text{co}} = 3.3_{-0.7}^{+2.8} M_{\odot}$. Since the value exceeds a conventionally accepted range of the maximum mass of the neutron star, it could be a single BH, or even a binary neutron star/BH. For simplicity, we assume that the inner

binary is near-circular and coplanar with the outer orbit, and set $m_{\text{giant}} = m_*$ and $m_{\text{CO}} = m_1 + m_2$; see Table 1. Then we apply the RV approximation formula so as to constrain the viable parameters for the possible inner binary.

Figure 2 plots a color contour map of K_{BBH} as a function of the mass ratio m_2/m_1 and the orbital period P_{in} of the possible inner binary for the 2M05215658+4359220 system. We compute the value of K_{BBH} from equation (3) using the parameters listed in Table 1. The color is coded according to the value of K_{BBH} that labels the contour curves.

The axis on the right indicates the semi-major axis ratio ($a_{\text{in}}/a_{\text{out}}$) corresponding to the orbital period P_{in} of the left axis. Note that the approximation formula is degraded towards the upper part of Figure 2. Indeed the three-body system becomes dynamically unstable if it satisfies (Mardling & Aarseth 2001)

$$\alpha > \left(\frac{a_{\text{in}}}{a_{\text{out}}} \right)_{\text{crit}} \equiv \frac{1 - e_{\text{out}}}{2.8} \left(\frac{(1 + m_3/(m_1 + m_2))(1 + e_{\text{out}})}{\sqrt{1 - e_{\text{out}}}} \right)^{-\frac{2}{5}} \approx 0.270. \quad (4)$$

Thus, the perturbation result completely breaks down there as indicated by the black area in Figure 2. Although the approximation formula is degraded for large ($a_{\text{in}}/a_{\text{out}}$), we can still conservatively estimate the semi-amplitude of RV variations in the allowed region of Figure 2.

Incidentally, the coalescence time of a circular compact binary t_{GW} via its GW emission is given by Peters (1964):

$$t_{\text{GW}} = \frac{5}{256} \frac{c^5 a_{\text{in}}^4}{G^3 m_{12}^2 \mu} \approx 1.88 \times 10^{11} \left(\frac{P_{\text{in}}}{\text{day}} \right)^{8/3} \left(\frac{m_{12}}{M_{\odot}} \right)^{-5/3} \text{ yrs}, \quad (5)$$

where $m_{12} = m_1 + m_2$, $\mu \equiv m_1 m_2 / m_{12}$. Equation (5) ensures that we can safely neglect the effect of GW emissions unless $P_{\text{in}} \ll 1$ days.

Considering no detection of anomalous RV variations by TRES beyond ~ 100 m/s, Figure 2 shows that an assumed inner coplanar circular binary is constrained to have orbital period less than a couple of weeks if the binary consists of an almost equal mass objects.

Assuming a planet orbiting around the red giant with its stellocentric semi-major axis a_{pl} , the orbital period of planet P_{pl} is obtained as

$$P_{\text{pl}} \approx 11 \text{ days} \left(\frac{a_{\text{pl}}}{30 R_{\odot}} \right)^{3/2} \gtrsim 11 \text{ days}. \quad (6)$$

Thus, the period of RV variations by a planet needs to be longer than 11 days. On the other hand, the period of variations by an inner binary is constrained to be shorter than $P_{\text{in}}/2 \sim 13/2$ days from Figure 2. Since the outer orbiting star is a red giant of a radius $\sim 30 R_{\odot}$ (see Table 1), we can basically break the degeneracy between an inner binary and an S-type circumbinary planet even if the periodic RV variation is detected.

3. STRATEGY TO SEARCH FOR AN INNER BINARY: CASE FOR A COPLANAR CIRCULAR TRIPLE

In this section, we concentrate on coplanar circular triples before considering coplanar eccentric systems in the next section. The main purpose of this section is to describe our methodology to

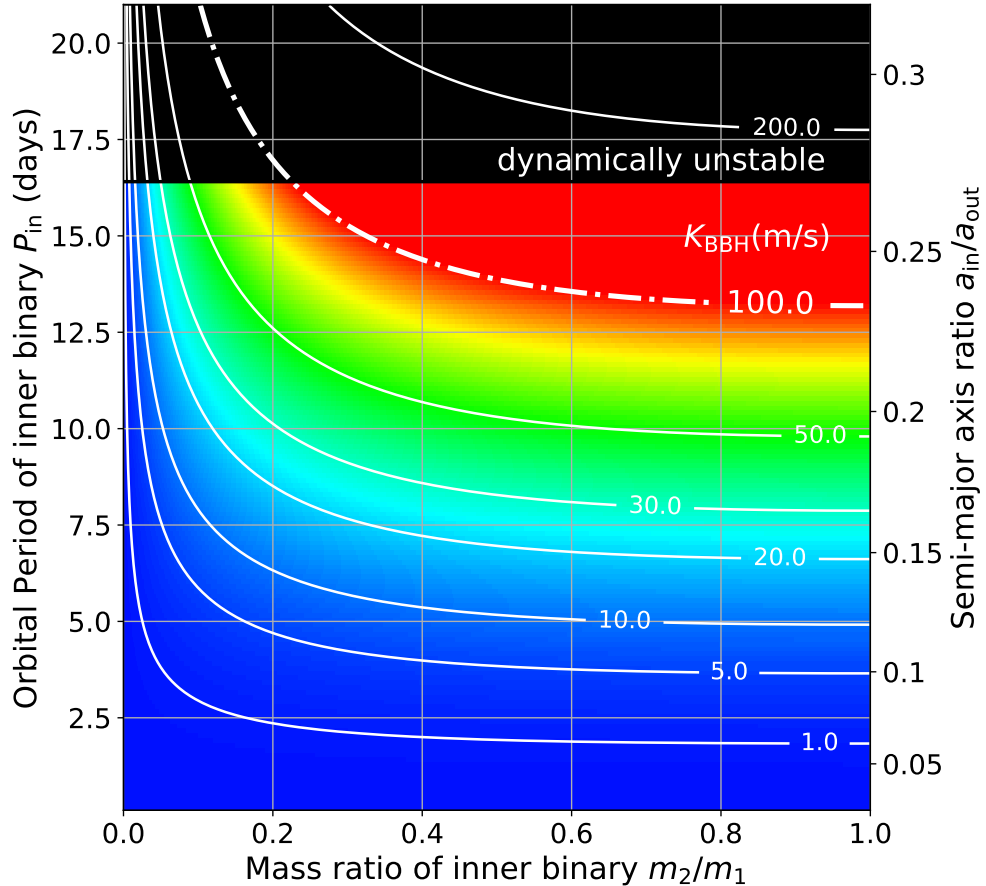


Figure 2. Characteristic semi-amplitude of RV variations K_{BBH} induced from a hypothetical inner binary in 2M05215658+4359220. Each contour curve is labeled by the value of K_{BBH} in units of m/s. The black region specifies the dynamically unstable region calculated using [Mardling & Aarseth \(2001\)](#).

search for a possible inner binary in a star – BH system, and also to check the accuracy of our numerical simulation against the analytic solution. Since there are many parameters characterizing a triple system, we cannot explore an entire parameter space. Instead, we fix a fiducial model, and examine the feasibility of our method for the model.

Table 2 summarizes the initial values of parameters in our fiducial model. As before, we use subscripts “in” and “out” to denote the parameters for inner and outer orbits, respectively. We adopt a $1 M_{\odot}$ star as the tertiary for simplicity. Also we assume a relatively large value for $(a_{\text{in}}/a_{\text{out}})$ within the dynamically stable range ([Mardling & Aarseth 2001](#)). In the present section, we consider a circular system, and set inner and outer eccentricities $e_{\text{in}}, e_{\text{out}}$ to 10^{-5} . We vary this value when we consider eccentric systems later in section 4. As a reference, Table 3 lists the predicted values for orbital motions calculated from equation (1).

Then, we perform N-body simulations for the coplanar circular triple with initial conditions in Table 2, using a public N-body package REBOUND ([Rein & Liu 2012](#)). We use WHFast integrator ([Rein & Tamayo 2015](#)), which is one of the fast and accurate symplectic integrators, and set the calculation time interval to be $10^{-6} \text{ yr}/2\pi$. We output the RV data in 0.1-day cadence over 800 days in total.

parameter	initial value
semi-major axis a_{in}	1.0 au
semi-major axis a_{out}	4.0 au
mass of the primary m_1	10 M_{\odot}
mass of the secondary m_2	10 M_{\odot}
mass of the tertiary m_*	1 M_{\odot}
inclinations $I_{\text{in}}, I_{\text{out}}$	90 deg
arguments of pericenter $\omega_{\text{in}}, \omega_{\text{out}}$	0 deg
longitudes of ascending node $\Omega_{\text{in}}, \Omega_{\text{out}}$	0 deg
true anomaly f_{in}	30 deg
true anomaly f_{out}	120 deg

Table 2. Initial values of parameters for our fiducial triple.

parameter	value
orbital period P_{in}	81.7 days
orbital period P_{out}	638 days
semi-amplitude of Keplerian RV K_0	65.0 km/s
variation period (2nd term in eq.(1)) P_{var1}	50.5 days
variation period (3rd term in eq.(1)) P_{var2}	43.6 days
half an inner period $P_{\text{in}}/2$	40.9 days
characteristic semi-amplitude of variations K_{BBH}	130.1 m/s

Table 3. Predicted values for orbital motions calculated from equation (1) and Table 2.

Since we are looking for a tiny RV variation relative to a much larger Keplerian component, we need to determine the base-line Keplerian motion accurately and subtract it from the total RV. Although it may seem a trivial and straightforward procedure, it is not the case in reality.

Figure 3 illustrates an example of RV residuals. First we compute the total RV signal of the tertiary star numerically. Since we know the initial values of the input parameters (Table 2), we subtract the first-term in the right-hand-side of equation (1) assuming $P_{\text{out}} = 638$ days and $e_{\text{out}} = 0$ (Table 3) from the total RV signal. The result is plotted as a black dashed line, which exhibits a large-amplitude modulation of a period close to P_{out} . This discrepancy comes from the fact that the orbital period of the outer star is indeed affected by the motion of the inner binary. In other words, P_{out} is not a constant unlike as assumed in the approximate formula, equation (1).

Therefore, we next fit the total RV signal using a RV fitting code `RadVel` (Fulton et al. 2018), and determine the best-fit Keplerian motion locally over the over 800 days. In doing so, we fix a constant motion (γ velocity) and neglect the RV jitters. The resulting best-fit values are summarized in Table 4. The blue line in Figure 3 is the RV residual after removing the *locally fitted* Keplerian component with $\tilde{P}_{\text{out}} \approx 619.3$ days and $\tilde{e}_{\text{out}} \approx 0.016$. It is in good agreement with the RV variation induced by an inner binary, the second and third terms in equation (1), which is plotted as a red line in Figure 3.

parameter	value
orbital period \tilde{P}_{out}	619.3041 days
time of conjunction $\tilde{T}_{\text{j,out}}$	566.12833 days
eccentricity \tilde{e}_{out}	0.01565794
pericenter argument $\tilde{\omega}_{\text{out}}$	-1.007588 rad
the semi-amplitude of RV $\tilde{K}_0 \sin \tilde{I}$	65931.314 m/s

Table 4. Best-fit parameters estimated with *RadVel* for our fiducial coplanar circular triple. Tildes on each variable indicates that they are fitted from the total RV curve over 800 days.

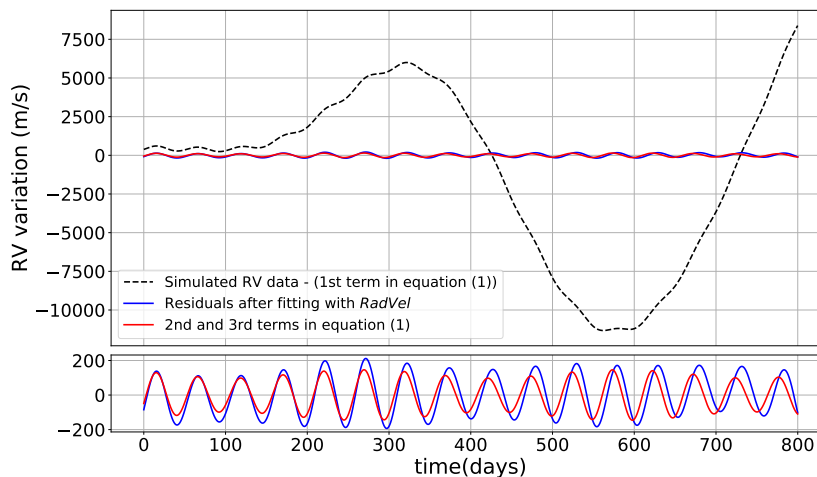


Figure 3. Comparison between the analytic approximation (the second and third terms of equation (1)) and the numerically computed RV residual; see the main text for detail

The above result implies that the removal of the accurate Keplerian component from the total RV signal is crucial to extract the RV variations due to an inner binary. The good agreement between our numerical result and the analytic formula for the RV variation simultaneously justifies the robustness of our methodology proposed here. There is a tiny discrepancy between the blue and red lines, but it is likely due to the limitation of the perturbative approximation, because our fiducial set of parameters are not fully in the perturbative regime.

Therefore, in what follows, we use fitting with *RadVel* to determine the base-line Keplerian component, and define the residuals as RV variations.

4. MOCK OBSERVATION OF A COPLANAR ECCENTRIC TRIPLE

This section considers effects of eccentricities for coplanar triples. Although [Morais & Correia \(2011\)](#) provide analytic perturbative RV formulae even for non-coplanar eccentric cases, the applicability of the result is limited by the validity of the perturbative approach. Also the formulas are fairly complicated and it is not easy to understand the overall behavior of RV variations. Therefore, we first provide examples for the predicted RV variations from numerical simulations, and then perform mock observations including noise and finite sampling. Finally we discuss the feasibility of the detection of an inner binary based on our methodology.

4.1. *RV variations for coplanar eccentric triples*

For definiteness, we consider four cases of different eccentricities: $(e_{\text{in}}, e_{\text{out}}) = (10^{-5}, 10^{-5})$, $(10^{-5}, 0.2)$, $(0.1, 10^{-5})$, and $(0.1, 0.2)$. The other parameters are fixed as those listed in Table 2. As in section 3, we generate the RV data in 0.1-day cadence over 800 days using `REBOUND`, and extract the base-line Keplerian motion fitted with `RadVel`

Figure 4 shows the RV variations (*left*) and the corresponding Lomb-Scargle (LS) periodogram (*right*). The LS periodograms are calculated using a community-developed core Python package for Astronomy, `Astropy` (Astropy Collaboration et al. 2013, 2018).

The RV variation for a coplanar circular triple exhibits a clear periodic signal as shown in the top-left panel of Figure 4. According to equation (1), the variation should have two distinct frequencies $\nu_{\text{var1}} \equiv 2\nu_{\text{in}} - \nu_{\text{out}}$, and $\nu_{\text{var3}} \equiv 2\nu_{\text{in}} - 3\nu_{\text{out}}$, corresponding to

$$P_{\text{var1}} = \frac{P_{\text{in}}P_{\text{out}}}{2P_{\text{out}} - P_{\text{in}}}, \quad (7)$$

and

$$P_{\text{var3}} = \frac{P_{\text{in}}P_{\text{out}}}{2P_{\text{out}} - 3P_{\text{in}}}, \quad (8)$$

respectively. The LS periodograms in the top-right panel of Figure 4 indicates that the RV variation that we compute numerically is dominated by the mode with $\sim 1/P_{\text{var3}} \approx 0.02 \text{ day}^{-1}$, and the mode with $\sim 1/P_{\text{var1}} \approx 0.023 \text{ day}^{-1}$ is barely visible. For comparison, we also computed the LS periodogram directly for the second and third terms of equation (1) with the same parameters and 0.1-day cadence over 800 days. We found that the secondary peak at ν_{var1} is not visible either, but correctly reproduced only when the total base-line duration is significantly larger than the 800 days we adopted here. Therefore, the identification of the two distinct modes due to an inner binary is very challenging in practice.

The LS periodograms also imply that non-zero eccentricities generate a variety of additional frequency modes in the LS periodograms, and that the value of the frequency ν_{var3} is fairly insensitive to e_{in} , but decreases as e_{out} increases. The sensitivity of the RV variation curve in time domain, instead of the LS periodogram, on e_{in} and e_{out} may be useful to estimate those eccentricities of the system. Thus we conclude that the presence of the inner binary itself can be inferred robustly. Also we find that the eccentricity is useful in distinguishing between the inner binary and the planetary signals as we discuss in section 5.

4.2. *Mock observations*

In order to examine the feasibility of our methodology to detect an inner binary, we perform mock observations of the RV signal including observational noise and finite sampling effect. If the tertiary star is a solar-type star located at $\sim 1 \text{ kpc}$, the apparent magnitude is around 15. According to Plavchan et al. (2015), the statistical RV error is at the level of a few tens of m/s with an ideal 10m telescope with ~ 1000 second exposure. While the noise is crucially dependent on the nature of the star, we neglect any systematic/non-Gaussian noise, and add 20 m/s Gaussian noise into the RV signal.

The observational cadence also affects the detectability of the inner binary. We consider two different cases; 10 and 30 data points randomly selected from one-day cadence data over 100 days.

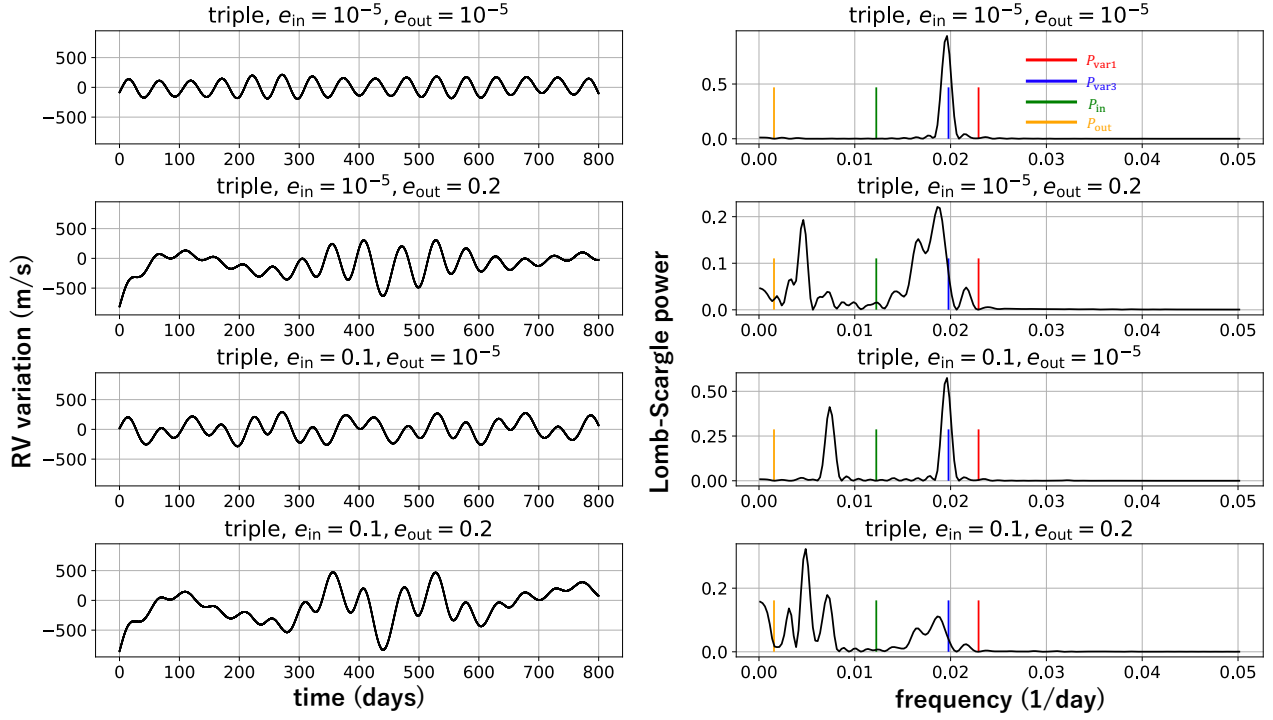


Figure 4. RV variations from numerical simulations: RV variation curves (*left*) and their Lomb-Scargle periodograms (*right*). For reference, the vertical lines in the right panel indicate relevant frequencies of the systems calculated from Table 3.

In both cases, we assume that the same cadence data are available for 600 days. Then we fit the data over 600 days with `RadVel` to extract the base-line Keplerian component, and obtain the RV residuals.

The results are shown in Figure 5 for the 30 percent sampling rate, and in Figure 6 for the 10 percent sampling rate. Blue lines in the left panels of Figures 5 and 6 correspond to the original RV variation curves of Figure 4. We note that we add the noise on the *total* RV curve, instead of the RV variation curve (blue lines). Thus the extracted Keplerian component is not exactly the same depending on the Gaussian noise. This is why the data points in the left panels of the two figures do not necessarily distribute around the blue lines. This clearly implies that an accurate determination and extraction of the base-line Keplerian component is crucial in our methodology.

Except for the limitation, Figures 5 and 6 indicate that the RV variations can clearly reveal the presence of the inner binary if the relevant short-cadence RV follow-up is performed. The LS periodograms in our mock data are very similar to the idealized cases shown in Figure 4; the peaks around the frequency $\nu_{\text{var}3}$ are fair robust even in the (modest) eccentricities we assumed here.

While the inner binary orbital period can be inferred relatively easily, it would be difficult to determine the mass ratio m_2/m_1 of the binary. As equation (3) indicates, the RV variations are more insensitive to the mass ratio than to the inner binary separation. Even a small uncertainty of the amplitude due to noise would affect the estimate of the mass ratio.

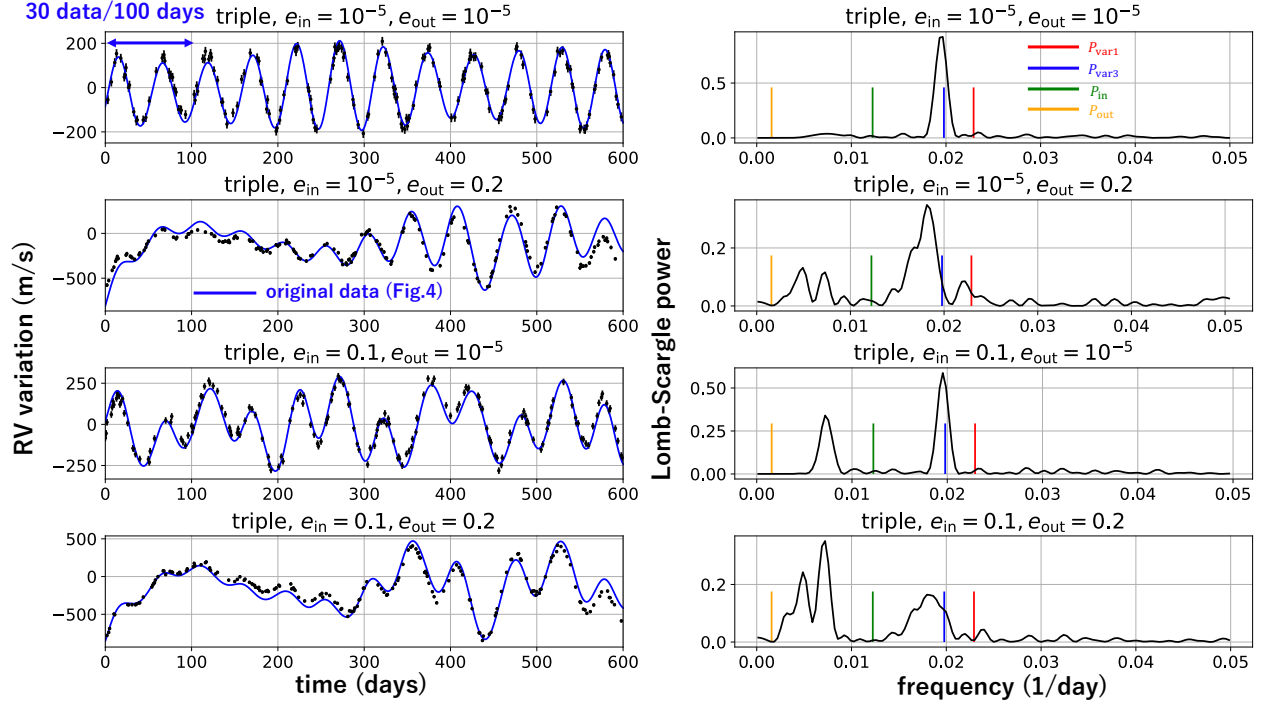


Figure 5. RV variation curves from mock observations of the original data plotted in Figure 4 and their LS periodograms. We sample 30 data points from each 100-days segment of the total RV data, add 20 m/s Gaussian noise, and extract the Keplerian component fitted to the 30×6 points over 600 days. Thin blue curves in the left panels correspond to the original data without noise plotted in Figure 4. The vertical lines in the right panels indicate relevant frequencies of the systems calculated from Table 3.

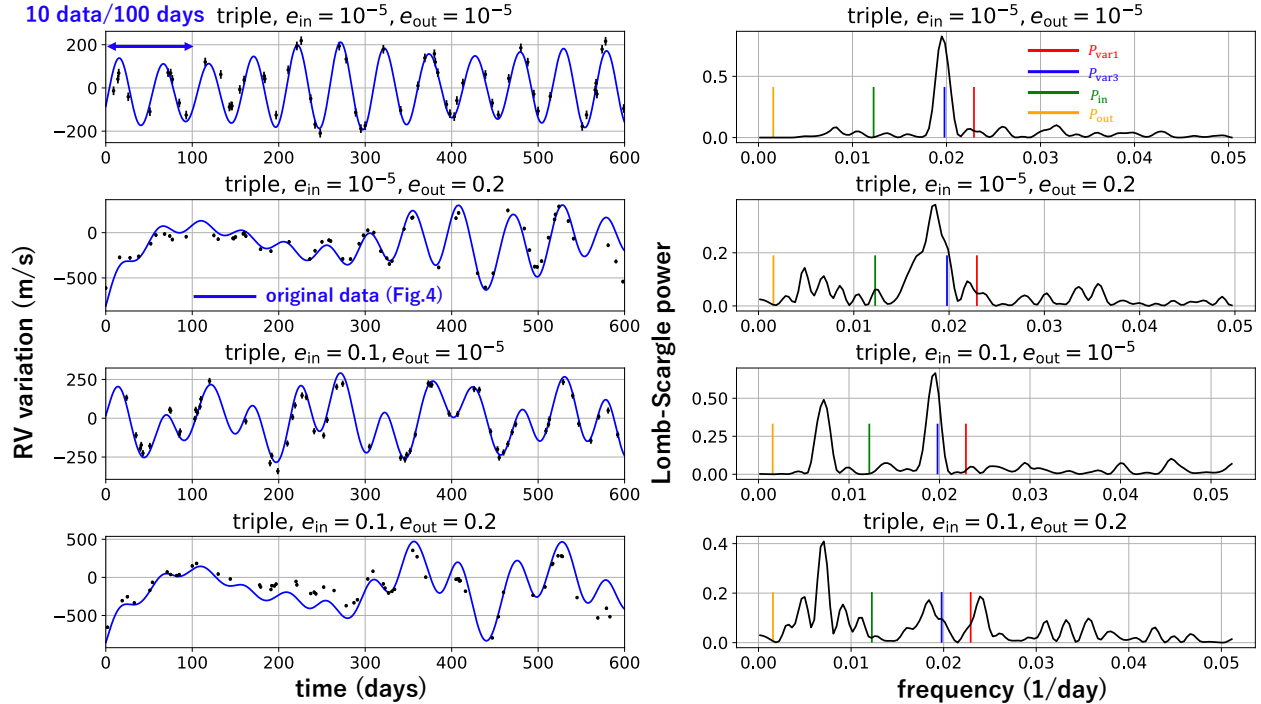


Figure 6. Same as Figure 5 but sampled 10 data points from each 100-days segment.

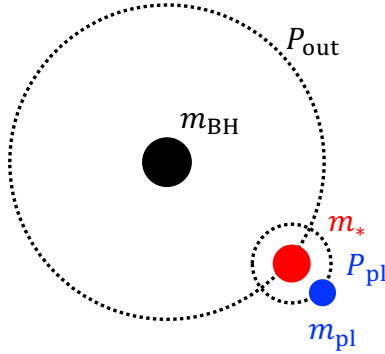


Figure 7. A binary consisting of a star and an unseen single BH.

parameter	initial value
semi-major axis a_{pl}	0.27 au
semi-major axis a_{out}	4.0 au
mass of the unseen companion m_{BH}	$20 M_{\odot}$
mass of the star m_*	$1 M_{\odot}$
mass of the planet m_{pl}	$2.7 M_{\text{J}}$
inclinations $I_{\text{pl}}, I_{\text{out}}$	90 deg
arguments of pericenter $\omega_{\text{pl}}, \omega_{\text{out}}$	0 deg
longitudes of ascending node $\Omega_{\text{pl}}, \Omega_{\text{out}}$	0 deg
true anomaly f_{pl}	30 deg
true anomaly f_{out}	120 deg

Table 5. Initial values of parameters for a fiducial binary with an S-type circumbinary planet orbiting around the star.

5. DEGENERACY WITH AN S-TYPE CIRCUMBINARY PLANET

As mentioned in sections 1 and 2, an S-type circumbinary planet (see Figure 7) produces a RV variation similar to that due to an inner binary. We examine the degree of a possible degeneracy by performing mock observations presented in section 4.

We consider the configuration of a star–BH binary system with a planet around a star. Following Appendix B, we choose a set of parameters for a planet (Table 5) so as to mimic the RV variations produced by our fiducial triple model (Table 2). We also consider non-zero eccentricities of the planetary and stellar orbits: $(e_{\text{pl}}, e_{\text{out}}) = (10^{-5}, 10^{-5}), (10^{-5}, 0.2), (0.1, 10^{-5}),$ and $(0.1, 0.2)$. While we choose the same set of values for $(e_{\text{in}}, e_{\text{out}})$ in subsection 4.2, e_{in} and e_{pl} do not have to be the same value in the two different pictures. We then perform the mock observations similar in section 4. We here consider the 30 percent sampling rate and examine if we can distinguish between the two pictures observationally.

Figure 8 shows the resulting RV variations (*left*) and the LS periodograms (*right*) for star–BH binaries with a planet orbiting around the star. As expected, a circular inner binary (top panels in Figure 5) is difficult to be distinguished from a star with a planet. The RV variation curves due to a planet are not so much affected by e_{pl} nor e_{out} , in contrast to their sensitivity due to an inner

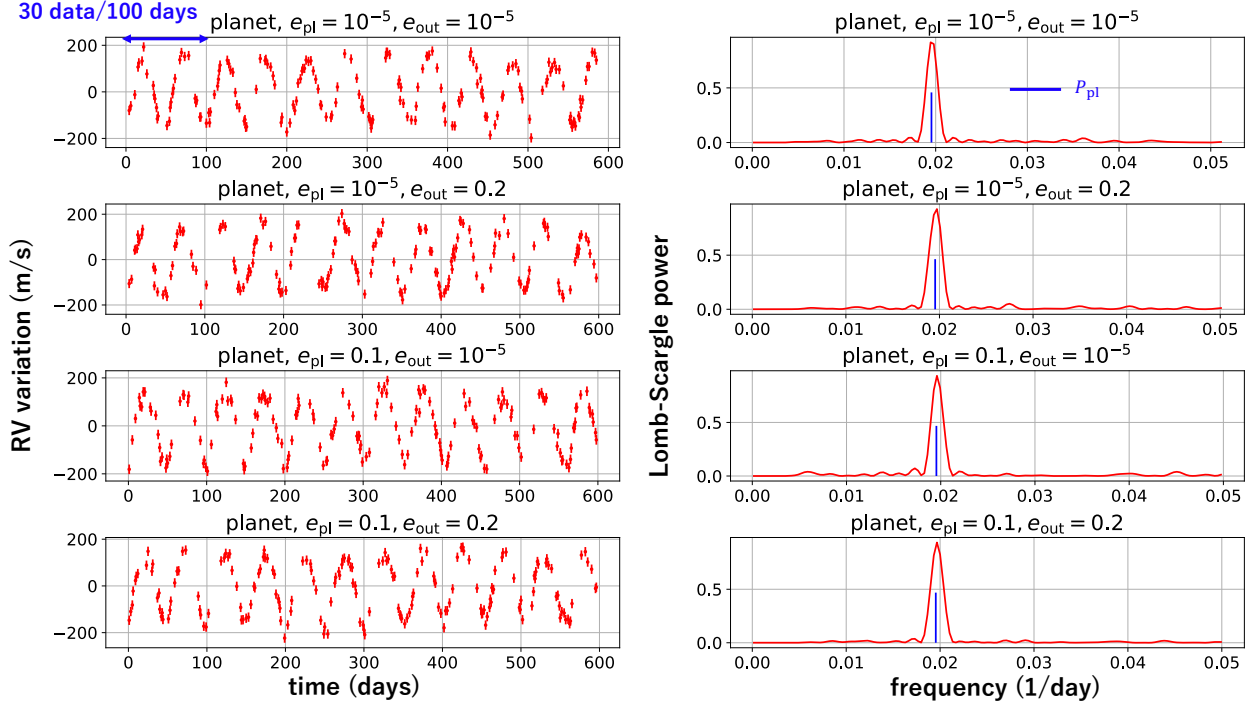


Figure 8. RV variations induced by an S-type circumbinary planet from mock observation based on the same parameters that are employed in Figure 5.

binary on e_{in} and e_{out} (Figure 5). Thus eccentricities of the inner binary is indeed helpful to break the degeneracy between the two models. In appendix B, we provide the parameter correspondence between the two possibilities for coplanar and circular systems.

6. SUMMARY

The LIGO-VIRGO detection of gravitational waves implies that the universe harbors a number of massive BBHs that have been dismissed in traditional astronomy. Since the GW emission from such BBHs is detectable only for the last few seconds before the final merger, their progenitors should be even more numerous and remain undetected as a population of unseen binaries with longer orbital periods.

We propose a methodology to detect such wider-separation BBHs from the motion of a star orbiting around them. The radial velocity of the tertiary star in a star – BBH triple system exhibits a periodic variation due to the orbital motion of the inner BBH. The variation signal is small compared with the Keplerian component of the stellar motion. Nevertheless it is comparable to, or even larger than, a typical amplitude of the radial velocities for observed exoplanetary systems. Thus such a velocity variation signal is indeed detectable if such star-BBH triples are identified.

There are several on-going projects that search for star – compact-object binaries based on astrometry, transit and radial-velocity surveys. They will soon discover a number of star-BH binary candidates, and a fraction of such binaries may be star-BBH triples, instead of mere binaries. Indeed a couple of binary systems, 2M05215658+4359220 (Thompson et al. 2019) and LB-1 (Liu et al. 2019), provide particularly interesting examples.

We have generated a series of mock radial velocity curves for coplanar systems, and showed that a short-period variation signal due to the inner BBH is detectable relatively easily as long as the star is sufficiently bright to allow for high-resolution spectroscopy, but that the mass ratio of the inner BBHs is difficult to estimate. The eccentricity of the tertiary star is useful in breaking the degeneracy between a planet orbiting the star and an inner BBH.

We find that a short-period variation in the 2M05215658+4359220 binary, if detected at all, should be due to the inner unseen binaries (neutron stars and/or BHs), since the red giant in the system cannot accommodate a planet with short orbital periods.

The discovery of LB-1 strongly indicated a presence of abundant star-BH binary systems in our Galaxy. LB-1 was originally claimed to contain a $68_{-13}^{+11}M_{\odot}$ unseen companion, which is intriguingly close to the total mass of several BBHs discovered by LIGO-VIRGO. Although subsequent studies (e.g. Abdul-Masih et al. 2019; El-Badry & Quataert 2019) suggested that the mass of the unseen companion is much smaller, the system still remains a promising target of the future RV follow-up. The current analysis focused on coplanar triples, but the inner and outer orbits are more likely to be mutually inclined. The extension of our methodology to LB-1 in a more general configuration will be examined and reported elsewhere.

Finally, we would like to emphasize that the methodology presented in this paper is no more a mere theoretical idea. It will find a realistic application in the near future that might unveil a hitherto unknown population of astronomical objects in a complementary manner to gravitational-wave observations.

ACKNOWLEDGMENTS

We would like to thank Alexandre C. M. Correia for letting us know of their important work on the degeneracy between the inner binary and the star with a planet, and Zheng Zheng for useful correspondences on LB-1. Simulations and analyses in this paper made use of REBOUND, RadVel, and Astropy. We gratefully acknowledge the support from Grants-in-Aid for Scientific Research by Japan Society for Promotion of Science (JSPS) No.18H01247 and No.19H01947, and from JSPS Core-to-core Program “International Network of Planetary Sciences”.

Software: Astropy (Astropy Collaboration et al. 2013, 2018), RadVel (Fulton et al. 2018), REBOUND (Rein & Liu 2012)

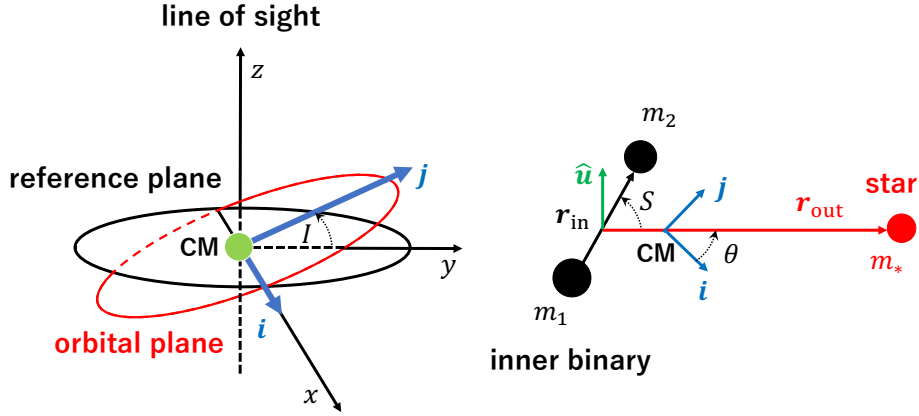


Figure 9. A schematic illustration of a triple system consisting of an inner binary and a tertiary star following [Morais & Correia \(2008\)](#). The left panel shows the common orbital plane of the inner binary and the tertiary star. The center of mass of the triple is denoted as CM. An observer is located along the z -direction with I being the inclination of the orbital axis measured by the observer. The right panel shows the definitions of orbital parameters of the system that are described in the main text.

APPENDIX

A. THE DERIVATION OF THE RV VARIATIONS INDUCED BY AN INNER BINARY

We here derive the equation (1) following [Morais & Correia \(2008\)](#). We consider a coplanar circular triple consisting of an inner binary ($\rho \equiv |\mathbf{r}_{\text{in}}|/|\mathbf{r}_{\text{out}}| \ll 1$) and a star orbiting around the binary (see the right panel of Fig.9). The Hamiltonian of the system to the second order of ρ is written as

$$\mathcal{H} = \frac{1}{2} \frac{\mathbf{p}_{\text{in}}^2}{\mu} + \frac{1}{2} \frac{\mathbf{p}_{\text{out}}^2}{\mu_*} - G \frac{m_1 m_2}{r_{\text{in}}} - G \frac{m_{12} m_*}{r_{\text{out}}} - G \frac{m_1 m_2 m_*}{r_{\text{out}} m_{12}} \rho^2 \frac{1}{2} (3 \cos^2 S - 1), \quad (\text{A1})$$

where $S \equiv \angle(\mathbf{r}_{\text{in}}, \mathbf{r}_{\text{out}})$, $m_{12} \equiv m_1 + m_2$, \mathbf{p}_{in} and \mathbf{p}_{out} are the momenta corresponding to \mathbf{r}_{in} and \mathbf{r}_{out} in terms of Jacobi coordinates, respectively. The reduced masses μ and μ_* are defined as

$$\mu \equiv \frac{m_1 m_2}{m_{12}} \quad \text{and} \quad \mu_* \equiv \frac{m_{12} m_*}{m_{12} + m_*}. \quad (\text{A2})$$

Using the Hamiltonian \mathcal{H} , the equations of motion are obtained from the canonical equations:

$$\dot{\mathbf{p}}_{\text{in}} = -\frac{\partial \mathcal{H}}{\partial \mathbf{r}_{\text{in}}} \quad \text{and} \quad \dot{\mathbf{p}}_{\text{out}} = -\frac{\partial \mathcal{H}}{\partial \mathbf{r}_{\text{out}}}. \quad (\text{A3})$$

Therefore, the explicit forms of equations of motion for the inner binary and outer star are

$$\ddot{\mathbf{r}}_{\text{in}} = -G \frac{m_{12}}{r_{\text{in}}^3} \mathbf{r}_{\text{in}} + G \frac{m_*}{r_{\text{out}}^3} (3\rho \cos S \mathbf{r}_{\text{out}} - \mathbf{r}_{\text{in}}) \quad (\text{A4})$$

and

$$\ddot{\mathbf{r}}_{\text{out}} = -G \frac{m_{12} + m_*}{r_{\text{out}}^3} \left[\left(1 + \frac{\mu}{m_{12}} \frac{\rho^2}{2} (-3 + 15 \cos^2 S) \right) \mathbf{r}_{\text{out}} - \frac{\mu}{m_{12}} 3\rho \cos S \mathbf{r}_{\text{in}} \right], \quad (\text{A5})$$

respectively.

The 0-th order solutions of equations (A4) and (A5) for a circular system are as follows:

$$\mathbf{r}_{\text{in}}^{(0)} = a_{\text{in}} \cos S \hat{\mathbf{r}}_{\text{out}} + a_{\text{in}} \sin S \hat{\mathbf{u}} \quad \text{and} \quad \mathbf{r}_{\text{out}}^{(0)} = a_{\text{out}} \hat{\mathbf{r}}_{\text{out}}, \quad (\text{A6})$$

where $S = S_0 + (\nu_{\text{in}} - \nu_{\text{out}})t$, and a_{in} and a_{out} are the semi-major axes of the inner and outer orbits, respectively, with S_0 being a constant phase determined by the initial positions. The mean motions ν_{in} and ν_{out} are defined as

$$\nu_{\text{in}} \equiv \sqrt{\frac{Gm_{12}}{a_{\text{in}}^3}} \quad \text{and} \quad \nu_{\text{out}} \equiv \sqrt{\frac{G(m_{12} + m_*)}{a_{\text{out}}^3}}. \quad (\text{A7})$$

In terms of the Cartesian coordinate on the orbital plane, unit vectors $\hat{\mathbf{r}}_{\text{out}}$ and $\hat{\mathbf{u}}$ are

$$\hat{\mathbf{r}}_{\text{out}} = \cos \theta \mathbf{i} + \sin \theta \mathbf{j} \quad \text{and} \quad \hat{\mathbf{u}} = -\sin \theta \mathbf{i} + \cos \theta \mathbf{j}, \quad (\text{A8})$$

where $\theta \equiv \theta_0 + \nu_{\text{out}}t$, and \mathbf{i} and \mathbf{j} are constant base vectors (see Figure 9), with θ_0 being a constant phase determined by the initial positions. Substituting equations (A6) - (A8) into the equation (A5), we obtain

$$\ddot{X} = -\frac{Gm_{12}}{a_{\text{out}}^2} \left[\left(1 + \frac{3}{4}\alpha^2 \frac{\mu}{m_{12}} \right) \cos \theta + \frac{9}{4}\alpha^2 \frac{\mu}{m_{12}} \cos 2S \cos \theta + \frac{3}{2}\alpha^2 \frac{\mu}{m_{12}} \sin 2S \sin \theta \right] \quad (\text{A9})$$

and

$$\ddot{Y} = -\frac{Gm_{12}}{a_{\text{out}}^2} \left[\left(1 + \frac{3}{4}\alpha^2 \frac{\mu}{m_{12}} \right) \sin \theta + \frac{9}{4}\alpha^2 \frac{\mu}{m_{12}} \cos 2S \sin \theta - \frac{3}{2}\alpha^2 \frac{\mu}{m_{12}} \sin 2S \cos \theta \right], \quad (\text{A10})$$

where X and Y are defined as $\mathbf{r}_{\text{out}} = X\mathbf{i} + Y\mathbf{j}$.

The solutions of these equations are written as

$$\begin{pmatrix} X \\ Y \end{pmatrix} = \begin{pmatrix} a_* \cos \theta \\ a_* \sin \theta \end{pmatrix} + \begin{pmatrix} \sin \theta & \cos \theta \\ -\cos \theta & \sin \theta \end{pmatrix} \begin{pmatrix} \delta_X \sin 2S \\ \delta_Y \cos 2S \end{pmatrix}, \quad (\text{A11})$$

where

$$a_* \equiv \frac{m_{12}}{m_{12} + m_*} \left(1 + \frac{3}{4}\alpha^2 \frac{\mu}{m_{12}} \right) a_{\text{out}}, \quad \delta_X \approx \frac{3}{8} \frac{\mu}{m_{12}} \alpha^4 a_{\text{out}} \quad \text{and} \quad \delta_Y \approx \frac{9}{16} \frac{\mu}{m_{12}} \alpha^4 a_{\text{out}}. \quad (\text{A12})$$

The above expressions for δ_X and δ_Y are derived on the assumption of $\nu_{\text{out}}/\nu_{\text{in}} \ll 1$.

The radial velocity V_{RV} is defined as

$$V_{\text{RV}} \equiv \dot{z} = \dot{Y} \sin I. \quad (\text{A13})$$

Therefore, we can write down the following RV approximation formula:

$$\begin{aligned} V_{\text{RV}} \approx & K_0 \left(1 + \frac{3}{4}\alpha^2 \frac{\mu}{m_{12}} \right) \sin I \cos[\nu_{\text{out}}t + \theta_0] \\ & - \frac{15}{16} K_{\text{BBH}} \sin I \cos[(2\nu_{\text{in}} - 3\nu_{\text{out}})t + (2S_0 - \theta_0)] \\ & + \frac{3}{16} K_{\text{BBH}} \sin I \cos[(2\nu_{\text{in}} - \nu_{\text{out}})t + (2S_0 + \theta_0)], \end{aligned} \quad (\text{A14})$$

where

$$K_0 \equiv \frac{m_{12}}{m_{12} + m_*} a_{\text{out}} \nu_{\text{out}} \quad \text{and} \quad K_{\text{BBH}} \equiv \frac{m_1 m_2}{(m_1 + m_2)^2} \sqrt{\frac{m_{12} + m_*}{m_{12}}} \alpha^{3.5} K_0. \quad (\text{A15})$$

B. CORRESPONDENCE OF PARAMETERS BETWEEN A TRIPLE AND S-TYPE CIRCUMBINARY PLANET

In section 5, we find that for a coplanar circular triple the RV variations are almost degenerate with those produced by an S-type circumbinary planet. If a star is a giant, we can sometimes rule out the degeneracy using the same way as for the system 2M05215658+4359220. However, this is not always applicable. Thus, we here consider a parameter correspondence for a coplanar circular case when we cannot distinguish these two possibilities.

The RV variations are basically characterized by its semi-amplitude K_{var} and period P_{var} . The latter is equal to P_{pl} and $P_{\text{in}}/2$ in the planet-star and inner BBH interpretations, respectively.

The semi-amplitude of RV variations induced by an inner binary is estimated from equation (3):

$$K_{\text{BBH}} = (2\pi G)^{1/3} \left(\frac{m_{123}}{m_{12}} \right)^{5/3} P_{\text{out}}^{-1/3} m_{123}^{1/3} \gamma^{-2} \left(\frac{P_{\text{in}}}{P_{\text{out}}} \right)^{7/3}, \quad (\text{B16})$$

where P_{out} is the orbital period of the outer star, $m_{12} = m_1 + m_2$, $m_{123} = m_{12} + m_*$, and $\gamma \equiv \left(\sqrt{m_2/m_1} + \sqrt{m_1/m_2} \right)$.

On the other hand, the semi-amplitude of variations induced by a coplanar circular planet around the outer star is

$$K_{\text{pl}} = (2\pi G)^{1/3} P_{\text{pl}}^{-1/3} m_{\text{pl}} m_*^{-2/3}, \quad (\text{B17})$$

where m_{pl} is the mass of planet, and we assume that $m_{\text{pl}} \ll m_*$.

We cannot distinguish these two interpretations from observation if both of them induce the RV variations with similar amplitude and period. For this case, using equations (B16) and (B17), we can obtain the parameter correspondence considering $K_{\text{var}} = K_{\text{BBH}} = K_{\text{pl}}$, and $P_{\text{var}} = P_{\text{pl}} = P_{\text{in}}/2$:

$$m_{\text{pl}} = 2^{7/3} m_*^{2/3} \left(\frac{m_{12}}{m_{12} + m_*} \right)^{5/3} \gamma^{-2} (m_{12} + m_*)^{1/3} \left(\frac{P_{\text{var}}}{P_{\text{out}}} \right)^{8/3}. \quad (\text{B18})$$

Equation (B18) relates the parameters in the two different interpretations.

Figure 10 shows the parameter correspondence between m_{pl} in the planet-star interpretation and m_{12} in the inner BBH interpretation for $P_{\text{out}} = 100$ days. We assume that $m_2/m_1 = 1$ and $m_* = 1 M_{\odot}$. Given the values of the RV variation semi-amplitude and period, K_{var} (color-coded) and P_{var} (black contour), the corresponding values of m_{pl} and m_{12} can be read off from the figures.

The dotted area above the blue curve is excluded in the inner BBH picture from the instability of the triple. We use the dynamical stability criterion (Mardling & Aarseth 2001) (see equation (4)) to compute the region. The tiny black region is excluded by the instability of the planet orbiting the star. To compute the region, we adopt the following Hill instability criterion (e.g. Holman & Wiegert 1999; Barnes & O'Brien 2002):

$$a_{\text{pl}} > f \left(\frac{m_*}{3m_{12}} \right)^{1/3} a_{\text{out}} \left(\mu \equiv \frac{m_{12}}{m_{12} + m_*} \gtrsim 0.8 \right), \quad (\text{B19})$$

where $f = 0.36$ is derived from numerical simulations, and a_{pl} is the stellocentric semi-major axis of planet. Note that m_{12} is interpreted as the mass of a single BH in a planet-star picture. Figure 10 shows that most of regions accept both interpretations, indicating that a Hot Jupiter around a star in a star-BH binary system may mimic the RV variation induced by an inner binary in the system.

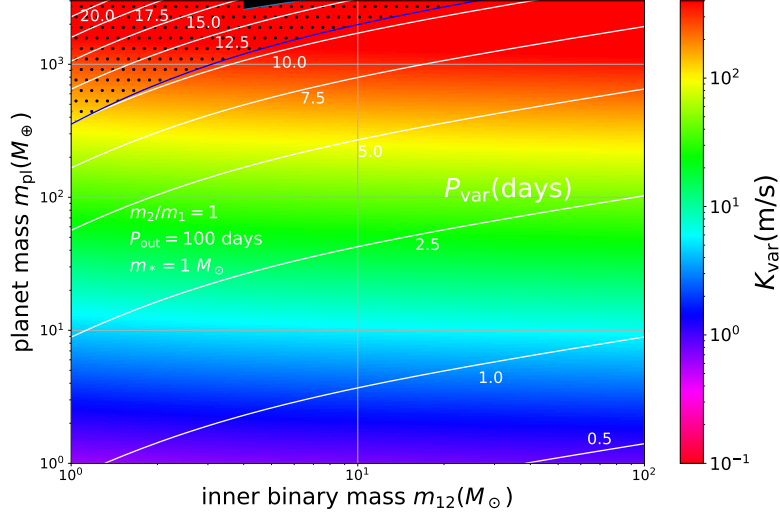


Figure 10. An example of the parameter degeneracy between the inner binary mass m_{12} and the planet mass m_{pl} that produce almost the same RV variation of a period P_{var} and a semi-amplitude $K_{|rmvar}$. We assume that a tertiary star of $1M_{\odot}$ orbits around an equal-mass BBH with an orbital period of $P_{\text{out}} = 100$ days. The dotted region excludes the inner BBH picture from the dynamical instability condition for the triple system according to [Mardling & Aarseth \(2001\)](#). The tiny black region excludes the planet picture from inequality ([B19](#)).

REFERENCES

- Abbott, B. P., Abbott, R., Abbott, T. D., et al. 2016, *Physical Review Letters*, 116, 061102
- Abdul-Masih, M., Banyard, G., Bodensteiner, J., et al. 2019, arXiv e-prints, arXiv:1912.04092. <https://arxiv.org/abs/1912.04092>
- Astropy Collaboration, Robitaille, T. P., Tollerud, E. J., et al. 2013, *A&A*, 558, A33
- Astropy Collaboration, Price-Whelan, A. M., Sipőcz, B. M., et al. 2018, *AJ*, 156, 123
- Barnes, J. W., & O’Brien, D. P. 2002, *ApJ*, 575, 1087
- Belczynski, K., Dominik, M., Repetto, S., Holz, D. E., & Fryer, C. L. 2012, ArXiv e-prints. <https://arxiv.org/abs/1208.0358>
- Belczynski, K., Holz, D. E., Bulik, T., & O’Shaughnessy, R. 2016, *Nature*, 534, 512
- Belczynski, K., Kalogera, V., & Bulik, T. 2002, *ApJ*, 572, 407
- Belczynski, K., Taam, R. E., Kalogera, V., Rasio, F. A., & Bulik, T. 2007, *ApJ*, 662, 504
- Bird, S., Cholis, I., Muñoz, J. B., et al. 2016, *Physical Review Letters*, 116, 201301
- Breivik, K., Chatterjee, S., & Larson, S. L. 2017, *ApJL*, 850, L13
- Dominik, M., Belczynski, K., Fryer, C., et al. 2012, *ApJ*, 759, 52
- . 2013, *ApJ*, 779, 72
- El-Badry, K., & Quataert, E. 2019, arXiv e-prints, arXiv:1912.04185. <https://arxiv.org/abs/1912.04185>
- El-Badry, K., & Rix, H.-W. 2018, *MNRAS*, 480, 4884
- Fulton, B. J., Petigura, E. A., Blunt, S., & Sinukoff, E. 2018, *PASP*, 130, 044504
- Hamers, A. S., Pols, O. R., Claeys, J. S. W., & Nelemans, G. 2013, *MNRAS*, 430, 2262
- Holman, M. J., & Wiegert, P. A. 1999, *AJ*, 117, 621
- Kawanaka, N., Yamaguchi, M., Piran, T., & Bulik, T. 2017, in *IAU Symposium*, Vol. 324, *New Frontiers in Black Hole Astrophysics*, ed. A. Gomboc, 41–42
- Kinugawa, T., Inayoshi, K., Hotokezaka, K., Nakauchi, D., & Nakamura, T. 2014, *MNRAS*, 442, 2963
- Kinugawa, T., Miyamoto, A., Kanda, N., & Nakamura, T. 2016, *MNRAS*, 456, 1093
- Liu, J., Zhang, H., Howard, A. W., et al. 2019, *Nature*, 575, 618

- Mardling, R. A., & Aarseth, S. J. 2001, *MNRAS*, 321, 398
- Mashian, N., & Loeb, A. 2017, *MNRAS*, 470, 2611
- Masuda, K., & Hotokezaka, K. 2019, *ApJ*, 883, 169
- Morais, M. H. M., & Correia, A. C. M. 2008, *A&A*, 491, 899
- . 2011, *A&A*, 525, A152
- O’Leary, R. M., Kocsis, B., & Loeb, A. 2009, *MNRAS*, 395, 2127
- Peters, P. C. 1964, *Physical Review*, 136, 1224
- Plavchan, P., Latham, D., Gaudi, S., et al. 2015, arXiv e-prints, arXiv:1503.01770.
<https://arxiv.org/abs/1503.01770>
- Portegies Zwart, S. F., & McMillan, S. L. W. 2000, *ApJL*, 528, L17
- Ransom, S. M., Stairs, I. H., Archibald, A. M., et al. 2014, *Nature*, 505, 520
- Rein, H., & Liu, S. F. 2012, *A&A*, 537, A128
- Rein, H., & Tamayo, D. 2015, *MNRAS*, 452, 376
- Rodriguez, C. L., Haster, C.-J., Chatterjee, S., Kalogera, V., & Rasio, F. A. 2016, *ApJL*, 824, L8
- Sasaki, M., Suyama, T., Tanaka, T., & Yokoyama, S. 2016, *Physical Review Letters*, 117, 061101
- . 2018, *Classical and Quantum Gravity*, 35, 063001
- Schneider, J., & Cabrera, J. 2006, *A&A*, 445, 1159
- Shen, R. F., Matzner, C. D., Howard, A. W., & Zhang, W. 2019, arXiv e-prints, arXiv:1911.12581.
<https://arxiv.org/abs/1911.12581>
- Spera, M., Mapelli, M., Giacobbo, N., et al. 2019, *MNRAS*, 485, 889
- Stephan, A. P., Naoz, S., Ghez, A. M., et al. 2016, *MNRAS*, 460, 3494
- Tagawa, H., Umemura, M., & Gouda, N. 2016, *MNRAS*, 462, 3812
- Thompson, T. A., Kochanek, C. S., Stanek, K. Z., et al. 2019, *Science*, 366, 637
- Toonen, S., Hamers, A., & Portegies Zwart, S. 2016, *Computational Astrophysics and Cosmology*, 3, 6
- Yamaguchi, M. S., Kawanaka, N., Bulik, T., & Piran, T. 2018, *ApJ*, 861, 21
- Ziegler, C., Law, N. M., Baranec, C., et al. 2018, *AJ*, 156, 259